A pilot investigation of the tricuspid valve annulus in newborns with hypoplastic left heart syndrome

Colton J. Ross, MS,[a] Elizabeth J. Trimble, MD,[b] Emily L. Johnson, PhD,[c] Ryan Baumwart, DVM,[d] Matthew A. Jolley, MD,[e] Arshid Mir, MD,[f] Harold M. Burkhart, MD,[b] and Chung-Hao Lee, PhD[a,g]

ABSTRACT

Objective: Hypoplastic left heart syndrome (HLHS) is a congenital disease characterized by an underdevelopment of the anatomical components inside the left heart. Approximately 30% of newborns with HLHS will develop tricuspid regurgitation, and it is currently unknown how the valve annulus mechanics and geometry are associated with regurgitation. Thus, we present an engineering mechanics-based analysis approach to quantify the mechanics and geometry of the HLHS-afflicted tricuspid valve (TV), using 4-dimensional echocardiograms.

Methods: Infants born with HLHS (n = 8) and healthy newborns (n = 4) had their TVs imaged, and the data were imported to 3D Slicer. The annular curves were defined at 5 points in the cardiac cycle. The geometry and deformation (strain) of the TV annulus were calculated to elucidate the mechanics of this critical structure and to compare them between neonates with and without HLHS.

Results: For the annular geometry, HLHS-afflicted newborns had significantly larger annular circumferences (20%-30%) and anteroposterior diameters (35%-45%) than the healthy patients. From a biomechanics' perspective, the HLHS patients had significantly smaller strains in the anterior segments (−0.1 ± 2.6%) during end-diastolic and end-isovolumetric relaxation (1.7 ± 3.0%) compared with the healthy counterparts (−13.3 ± 2.9% and 6.8 ± 0.9%, respectively).

Conclusions: The image-based analysis presented in this study may provide novel insights into the geometric and mechanistic differences in the TV annulus between the healthy and HLHS newborns. Future longitudinal studies of the biomechanics of TV annulus and other subvalvular structures may inform our understanding of the initiation and development of tricuspid regurgitation and the design of optimal repairs in this challenging population. (JTCVS Open 2022;10:324-39)

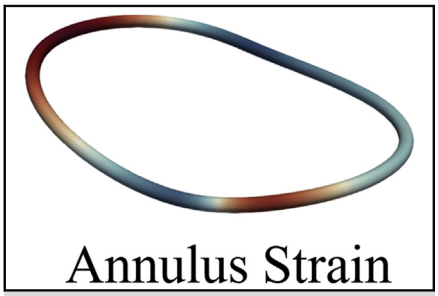

Computed TV annulus strain for patients with HLHS.

CENTRAL MESSAGE

The derived mechanics and geometry-based metrics of the tricuspid valve annulus in patients with HLHS can provide novel insight into the refinement of the timing for surgical interventions.

PERSPECTIVE

Hypoplastic left heart syndrome patients undergoing the staged palliation are susceptible to tricuspid valve regurgitation. Currently, there is limited information regarding the tricuspid valve annulus mechanics in this population, and an engineering-based analysis approach was performed to elucidate the distinct features (eg, mechanical strain) present in this unique congenital heart defect.

See Commentary on page 340.

From the [a]School of Aerospace and Mechanical Engineering, University of Oklahoma, Norman, Okla; Departments of [b]Surgery and [c]Pediatrics, University of Oklahoma Health Sciences Center, Oklahoma City, Okla; [d]Department of Aerospace and Mechanical Engineering, University of Notre Dame, Notre Dame, Ind; [e]Veterinary Clinical Sciences, College of Veterinary Medicine, Washington State University, Pullman, Wash; and [f]Departments of Anesthesiology and Critical Care and Pediatric Cardiology, Children's Hospital of Philadelphia, Philadelphia, Pa; [g]Institute for Biomedical Engineering, Science and Technology, University of Oklahoma, Norman, Okla.

Support provided by the Presbyterian Health Foundation Team Science Grant and the American Heart Association Scientist Development Grant (16SDG27760143). C.H.L. was supported in part by the IBEST-OUHSC Funding for Interdisciplinary Research and the OU Research Council. C.J.R. was supported in part by the National Science Foundation Graduate Research Fellowship (GRF 2020307284). M.A.J. and the 3D Slicer imaging tools used in this work were supported by National Institutes of Health R01HL153166. Financial support was provided by the University of Oklahoma Libraries' Open Access Fund.

Received for publication Sept 23, 2021; accepted for publication Feb 10, 2022; available ahead of print March 17, 2022.

Address for reprints: Chung-Hao Lee, PhD, School of Aerospace and Mechanical Engineering, University of Oklahoma, 865 Asp Ave, Felgar Hall 219C, Norman, OK 73019 (E-mail: ch.lee@ou.edu).

2666-2736

https://doi.org/10.1016/j.xjon.2022.02.015

Abbreviations and Acronyms

AP = anteroposterior
D_{AP} = anteroposterior diameter
D_{SL} = septal-lateral diameter
ED = end diastole
EIVC = end-isovolumetric contraction
EIVR = End-isovolumetric relaxation
ES = end systole
HLHS = hypoplastic left heart syndrome
IRB = institutional review board
r = Pearson correlation coefficient
RVP_{min} = minimum right ventricular pressure
TR = tricuspid regurgitation
TV = tricuspid valve
(X, Y, Z) = Cartesian coordinates

Video clip is available online.

Hypoplastic left heart syndrome (HLHS) is present in 1 of every 3841 births in the United States and is associated with a 20.6% mortality rate within the first 2 weeks of life.[1,2] Staged cardiac palliation surgery is the primary treatment method for neonates with HLHS; however, interstage mortality, postpalliation mortality, and tricuspid valve (TV) complications remain emerging challenges for this pediatric population.[3-5] For example, up to 32% of newborns develop significant tricuspid regurgitation (TR) by the second palliation stage,[6,7] which is associated with a relatively high mortality rate and suboptimal repair outcomes.[8,9] Patient characteristics with the presence and recurrence of TR have been documented, including early intervention (eg, younger, lower body weight) and abnormal valve architectures (eg, leaflet tethering).[6-8,10-16] These complications may be due to the increased afterload on the TV during the reconstructive palliations, subsequently resulting in valvular tissue remodeling to maintain tissue homeostasis.[17-19]

While these advancements facilitate a deeper understanding of the geometric abnormalities related to the presence of TR in patients with HLHS, there are currently no biomechanics-focused studies of the TV structures. Mechanical strain, caused by external constraints or loads (in this case due to right ventricular contraction and valve closure), is a geometric measure of deformation, representing the relative displacement between particles in a material body. Understanding the functional strains, together with other engineering mechanics metrics, is crucial for optimizing TV surgical techniques that can ideally prevent TR progression. Specifically, TV interventions, such as valvuloplasty, may be improved to better target the desired tissue homeostatic stress and strain to avoid adverse tissue remodeling and the subsequent disease worsening. To this end, we develop a mechanics-based TV annulus analysis pipeline to quantify and systematically analyze the clinical, geometric, and engineering mechanics metrics in

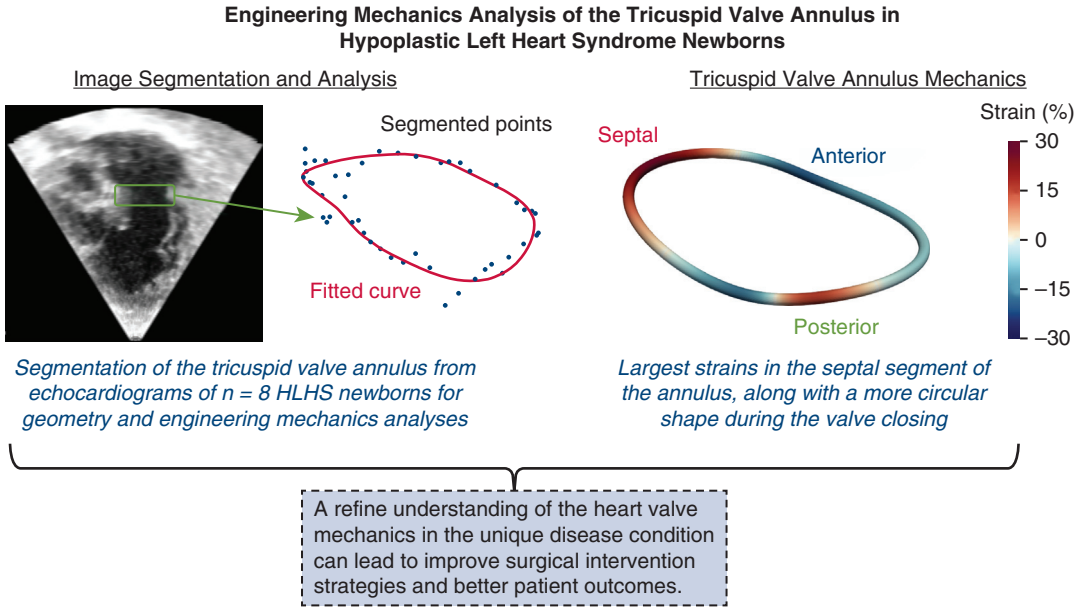

FIGURE 1. Overview of the study, including the echocardiogram image segmentation, mechanics-based analysis results, and the implications of our work. *HLHS*, Hypoplastic left heart syndrome.

HLHS-afflicted TVs (Figure 1). In this pilot study, we use this pipeline to analyze a cohort of 8 newborns with HLHS (n = 8) and 4 healthy newborns (n = 4), which can lay the foundation for future studies to identify the predictors of TV annulus mechanics associated with TR.

METHODS

This is a single-center study, reviewed and approved by the institutional review board (IRB) at the University of Oklahoma Health Sciences Center, for a retrospective (IRB no. 14112; obtained on December 8, 2021) enrollment of patients diagnosed with HLHS from July 2019 to present. Due to the retrospective nature of the study, patient consent was not required.

Study Population

The inclusion criteria for the 8 currently enrolled patients with HLHS were that they (1) have HLHS and (2) have no evidence of moderate or severe TR. Meanwhile, the inclusion criterion for another 4 healthy patients was the absence of cardiovascular disease or defects, and they were imaged for concerns, such as hypoxia or heart murmurs, but presented with normal cardiovascular function. Table 1 summarizes the characteristics of all 12 patients (eg, birth weight, gestational age).

Echocardiogram Imaging and Image Segmentation

Routine 4-dimensional full-volume transthoracic echocardiographic data for a full cardiac cycle was collected in the apical view (coronal scanning plane) using a Philips EPIQ ultrasound machine (Philips NV) equipped with 5-MHz and 7-MHz matrix-array transducers under our IRB-approved protocol, where none of the patients were under sedatives/medications during the imaging procedure. The acquired 4-dimensional echocardiographic imaging data was converted into a Cartesian Digital Imaging and Communications in Medicine (3DDCM) format in QLAB Cardiac Analysis software (Philips NV).[19] The corresponding Digital Imaging and Communications in Medicine files from the patient imaging were then imported to the 3D Slicer software using the SlicerHeart module for definition of the TV annulus using the 3 standard views—the axial, sagittal, and coronal planes (Figure 2).[15,19,20] For the subsequent geometrical and engineering mechanics-based analyses, we defined 5 key time points of interest over the cardiac cycle[20-22]:

- Right ventricular minimum pressure (RVP_{min}): The TV is open (ie, leaflets are not in contact), and the right ventricle is at the minimum volume.
- End diastole (ED): The time instant right before the coaptation of the TV leaflets.
- End-isovolumetric contraction (EIVC): The TV is closed (ie, TV leaflets are in contact), and the right ventricle is at the maximum volume.
- End systole (ES): The TV is closed, and the ventricular volume is at the minimum.
- End-isovolumetric relaxation (EIVR): The TV is closed, and the ventricular volume is at the minimum volume without a change in ventricular volume.

At each of the aforementioned time points, the (*X*, *Y*) locations of the 3 commissure regions were first identified on the axial plane, ie, the anteroseptal, the anteroposterior (AP), and the posteroseptal (PS) commissures (Figure 2, *A*). Then, the segmentation of the TV annulus was performed within the 3D Slicer software through manual segmentation of the TV leaflet hinge points (Figure 2, *B*). These leaflet hinge points were identified at every 8° to 9° of the TV annulus by rotation of the sagittal plane view about the centroid of the imaging viewpoint (Figure 2, *D*). Following segmentation, the (*X*, *Y*, *Z*) coordinates of the segmented TV annulus point clouds were exported for the geometry and mechanics analyses. To ensure the consistency and robustness of our overall manual image segmentation, all TV annulus segmentations were performed in consultation with multiple clinicians (eg, pediatric cardiologist and pediatric cardiac surgeon) at the Oklahoma Children's Hospital and Children's Hospital of Philadelphia.

Geometry- and Engineering Mechanics–Based Analyses for the TV Annulus

The (*X*, *Y*, *Z*) coordinates from the TV annulus point clouds (ie, a collection of segmentation points; Figure 3, *A*) were imported to MATLAB (MathWorks). Annulus curve fitting was performed using a moving least-squares algorithm,[23,24] from which we retrieved 300 uniformly spaced material points (the number of material points was chosen to yield convergent strain, strain rate, and curvature) for the subsequent analyses. Note that we defined the 0° angle as the location of the AP commissure (Figure 3, *B*) and the positive angle as the clockwise rotation around the annulus circumference from 0° to 360°.

TABLE 1. Patient characteristics for the newborns with HLHS and healthy newborns considered in this study

Patient ID	Race	Sex	Birth weight/ height	Gestational age	Diameter of ascending aorta	TAPSE	RVFAC (%)	HLHS subtype
HLHS newborns								
1	Hispanic	Male	2790 g/46 cm	36 + 0/7 wk	0.29 cm ($z = -3.44$)	8.0 mm	44	MS/AoS
2	Caucasian	Male	3020 g/48.5 cm	37 + 1/7 wk	0.20 cm ($z = -4.77$)	8.5 mm	40	MS/AoA
3	Caucasian	Male	3310 g/52 cm	38 + 2/7 wk	0.16 cm ($z = -5.17$)	8.4 mm	41	MS/AoA
4	Caucasian	Male	3350 g/49 cm	38 + 1/7 wk	0.23 cm ($z = -4.73$)	8.0 mm	44	MS/AoS
5	Caucasian	Male	3180 g/52 cm	38 + 4/7 wk	0.32 cm ($z = -3.93$)	9.0 mm	45	MS/AoS
6	Unknown	Female	2700 g/49 cm	39 + 2/7 wk	0.40 cm ($z = -3.07$)	8.0 mm	43.8	MS/AoS
7	Caucasian	Female	2780 g/47.5 cm	38 + 5/7 wk	0.18 cm (z = N/A)	8.5 mm	37	MA/AoA
8	Hispanic	Male	3350 g/47.8 cm	39 + 1/7 wk	0.22 cm ($z = -4.76$)	6.5 mm	40	MA/AoA
Healthy newborns								
9	Hispanic	Female	1670 g/42.5 cm	33 + 3/7 wk	N/A	10.5 mm	55	N/A
10	Hispanic	Male	3575 g/55.5 cm	40 + 3/7 wk	N/A	10.7 mm	45	N/A
11	Unknown	Male	2260 g/45 cm	32 + 5/7 wk	N/A	8.7 mm	40	N/A
12	Caucasian	Male	2960 g/50 cm	39 + 4/7 wk	N/A	13.3 mm	62	N/A

Note that the diameter of the ascending aorta, RVFAC, and TAPSE scores were not measured in the healthy patients. *HLHS*, Hypoplastic left heart syndrome; *TAPSE*, tricuspid annular plane systolic excursion; *RVFAC*, right ventricular fractional area change; *MS*, mitral stenosis; *AoS*, aortic stenosis; *AoA*, aortic atresia; *N/A*, not available.

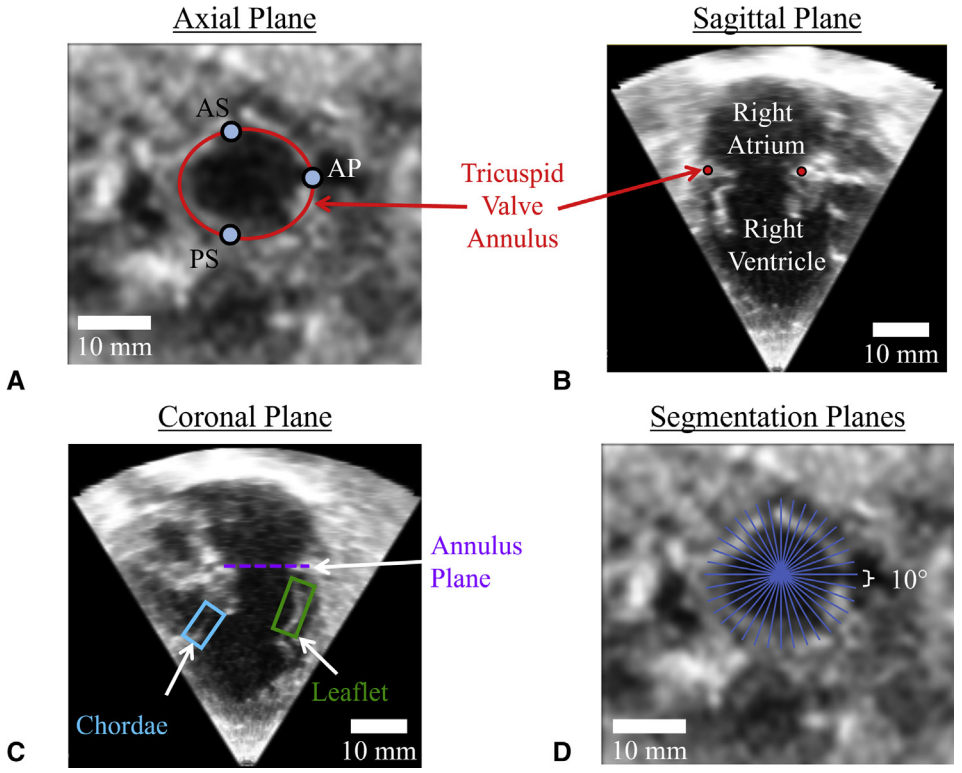

FIGURE 2. Four-dimensional transthoracic echocardiographic data from a representative newborn with HLHS (patient #1): (A) axial plane, (B) sagittal plane, and (C) coronal plane. D, Illustration of our image segmentation of the TV annulus. *HLHS*, Hypoplastic left heart syndrome; *TV*, tricuspid valve; *AS*, anteroseptal; *AP*, anteroposterior; *PS*, posteroseptal.

After annulus curve fitting, the typical clinical and geometric indices were quantified,[18] including: (1) the 2 primary annulus diameters: the AP diameter D_{AP} and the septolateral (SL) diameter D_{SL} (Figure 3, *B*), (2) the annular height (Figure 3, *C*), and (3) the bending angle, which is defined as the angle between the best fit planes of the flat region and the elevated region (*the flat region* is composed of the posterior annulus and the bordering half of the bisected septal annulus region, whereas *the elevated region* consists of the anterior annulus and the neighboring half of the bisected septal region) (Figure 3, *C*). We also determined other geometry-based metrics of interest, including the circumference, the annulus area, which is approximated by the sum of the area of triangles delimited by any 2 adjacent material points and the centroid of the annulus curve,[25] and the sphericity, which is calculated by D_{AP}/D_{SL}.

In addition, the biomechanical metrics were determined using the material points from the fitted curve. Herein, we defined RVP_{min} as the reference configuration, as it is the time point in the cardiac cycle closest to a *stress-free* reference configuration.[26] The annulus strains associated with each material point i located at (X_i, Y_i, Z_i), were computed as the changes in segment lengths between the RVP_{min} and the subsequent time points (the direction of strain is along the tangential direction of the annulus curve) (Figure 3, *A*). Thereafter, the strain rate was calculated as the difference in strain between the reference configuration and the subsequent time points per unit time (in seconds). We also quantified the curvature and the relative curvature (ie, the difference in curvature between the RVP_{min} and the subsequent time points).[27] A representative illustration of the spatial variations in the strain, strain rate, and curvature, between EIVC and RVP_{min} are shown in Figure 3, *D*. For more details on the moving least-squares curve fitting and the subsequent biomechanics-based quantifications, we refer the readers to Appendix 1.

Statistical Analysis

Normally distributed data was reported as the mean ± standard error of the mean and non-normal data as the median [the interquartile range]. For comparisons between patients, annular area measurements were first normalized by the body surface area, whereas the linear measurements were normalized by $\sqrt{BSA}$.[15] Herein, the body surface area was estimated using Haycock's formula.[28] Statistical comparisons were performed between the newborns with HLHS and healthy newborns: normal data via Student's *t* test (with Welch's correction in the case of unequal variances), and non-normal data via Wilcoxon rank-sum test. To analyze trends between the clinical measurements of patient right ventricular function and the TV geometries, we analyzed the Pearson's correlation coefficient (r).

Remark 1. Note that this study is a pilot investigation, and the statistical comparisons performed provide preliminary insights into the differences between newborns with HLHS and healthy ones. Future studies with larger cohorts will be required for more conclusive findings.

RESULTS

TV Annulus Geometric Features in Newborns With HLHS

From the perspective of geometry, we observed distinct changes in the TV annulus during the cardiac cycle for the newborns with HLHS (Figure 4 and Figure E1).

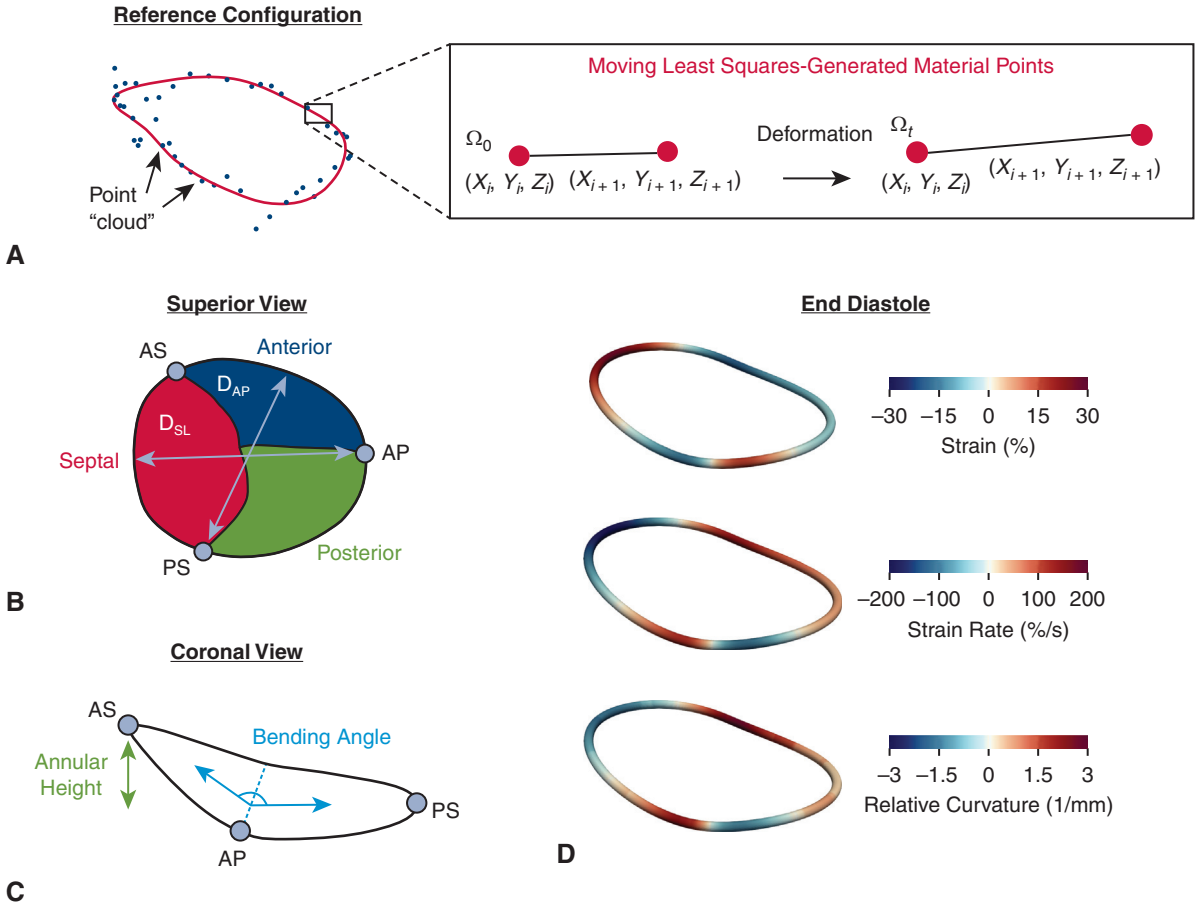

FIGURE 3. A, Visual description of the moving least-squares curve fitting to obtain a smoothed representation of the TV annulus. B, Schematic of the 2 diameters of the TV annulus: D_{SL} and D_{AP}. C, Illustration of the calculations of the annular height and the annulus bending angle. D, Representative annulus contours from patient #1 with HLHS at end diastole, showing the strain, strain rate, and relative curvature. *TV*, Tricuspid valve; D_{SL}, septal-lateral diameter; D_{AP}, anteroposterior diameter; *HLHS*, hypoplastic left heart syndrome; *AS*, anteroseptal; *AP*, anteroposterior; *PS*, posteroseptal.

Specifically, D_{AP} decreased during the leaflet coaptation (EIVC) by –12.9 ± 4.0%, whereas the trends for D_{SL} were less consistent, with one half of patients demonstrating an increase in D_{SL} (6.6%-45.7%), whereas the remaining patients exhibiting a decreased D_{SL} during EIVC (−3.6% to −18.5%). These changes were reflected in the sphericity and the annular area. For sphericity, nearly all patients (except patient #4) had an elliptical annulus shape (sphericity >1.0) at RVP_{min}, then becoming more circular throughout the cardiac cycle (ie, sphericity ≈ 1.0). For annular area, we found decreases between RVP_{min} and EIVC for all but one of the patients with HLHS (–42.1% to −6.8%), and a 13.0% increase for patient #7, who had a restrictive atrial septal defect. In contrast, the circumference remained relatively constant for each patient (variations within ±10% throughout the cardiac cycle).

The bending angle and annular height provide insights into the changes in the out-of-plane "saddleness" of the TV annulus. Specifically, we found the annulus to be flatter in the relaxed state (RVP_{min}, 166.2° [22.2°]) and more "bent" at valve closure (EIVC, 143.9° [8.1°]). We also noted an 8.2% to 87.7% increase in the annular height for 3 of the 8 newborns with HLHS at EIVC, whereas the remaining 5 patients showed a decrease in the annular height of –1.6% to –36.5%. In contrast, the quantified geometric changes for the healthy newborns are shown in Figure 5 and Figure E2.

Analyzing the patient right ventricular function data (Table 1), we observed moderate-to-strong correlations of the right ventricular fractional area change to the quantified geometric indices: D_{AP} ($-0.78 < r < -0.44$), D_{SL} ($-0.75 < r < -0.03$), area ($-0.57 < r < -0.36$), bending angle ($-0.55 < r < 0.81$), height ($0.22 < r < 0.67$), and sphericity ($-0.74 < r < 0.22$), whereas the right ventricular fractional area change was weakly correlated with the mechanical strain and strain rate along with a moderate correlation with the curvature in the septal segment

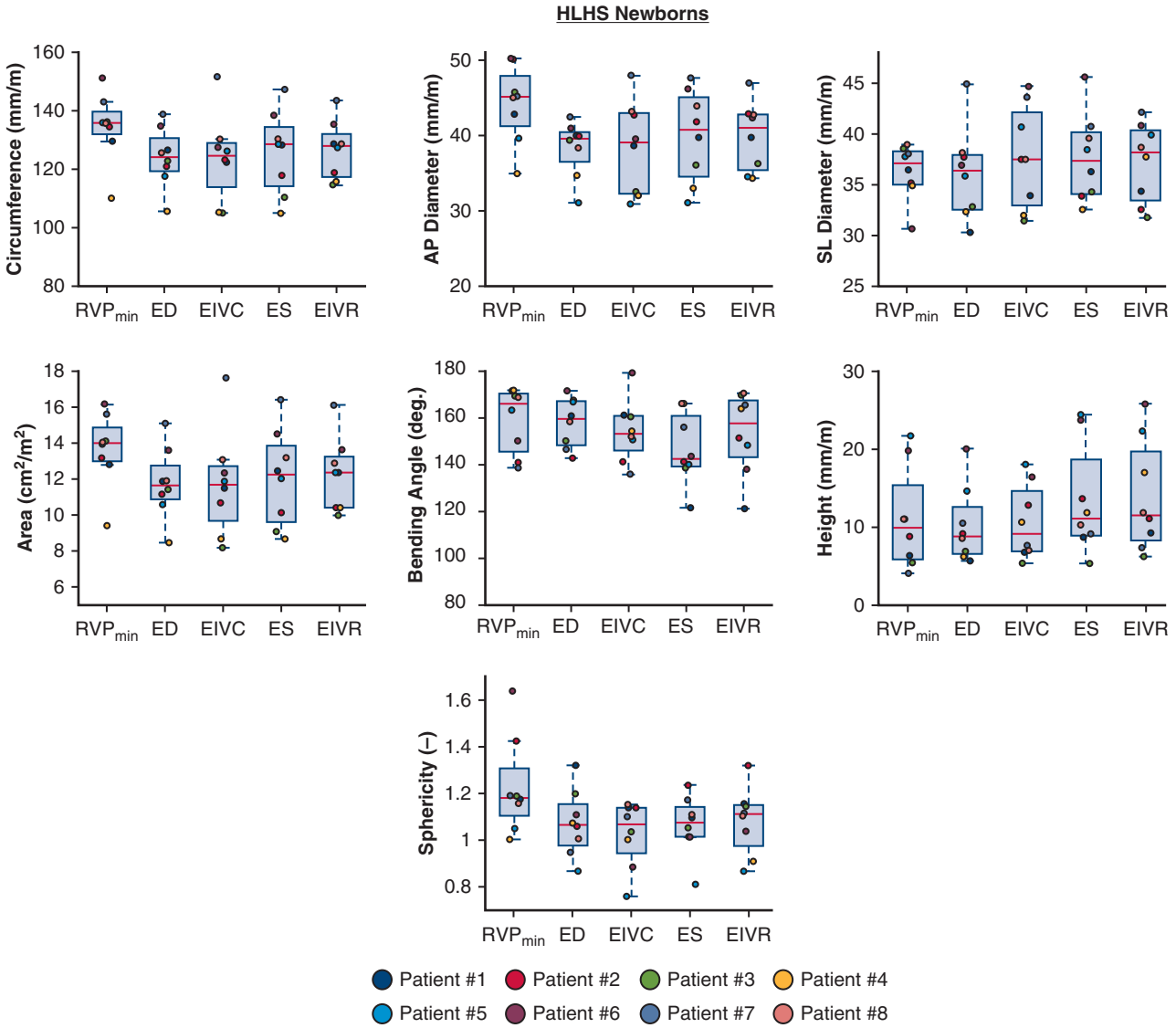

FIGURE 4. Key TV annulus clinical metrics for all newborns with HLHS (n = 8) at the selected time points over the cardiac cycle *solid red line*: the median, the bounding box: the 25th to 75th percentiles, the *whiskers*: extension between the maximum and minimum nonoutlier datapoints. Individual patient data points at each time point are visualized with jittering for improved visual clarity. *TV*, Tricuspid valve; *HLHS*, hypoplastic left heart syndrome; *RVP_{min}*, minimum right ventricular pressure; *ED*, end diastole; *EIVC*, end-isovolumetric contraction; *ES*, end systole; *EIVR*, end-isovolumetric relaxation; *SL*, septal-lateral; *AP*, anteroposterior.

($0.57 < r < 0.66$). In addition, there were moderate-to-strong correlations between the diameter of the ascending aorta and the annular height ($0.71 < r < 0.86$) and the strain in the posterior segment ($0.36 < r < 0.76$).

TV Annulus Mechanics for Newborns With HLHS

The spatial variations of the computed annulus strain around the circumference at each of the analyzed time points for one representative patient (ie, patient #1) are shown in Figure 6, whereas the computed annular strain, strain rate, and relative curvature across all patients are presented in Figure 7, Figure E3, and Figure E4, respectively. Video animations depicting the annulus shape and strains throughout the cardiac cycle for each patient (HLHS and healthy) are provided in Videos 1-12.

From the representative patient, we observed the largest compressive strains in the posterior annulus (a maximum strain of –8.8% at ED), whereas the anterior segment underwent the smallest strain throughout the cardiac cycle (<5% on average). Similarly, across all patients, we found the largest strains in the posterior and septal segments (–5.7 ± 2.2% and –8.7 ± 3.8% at ED, respectively), and

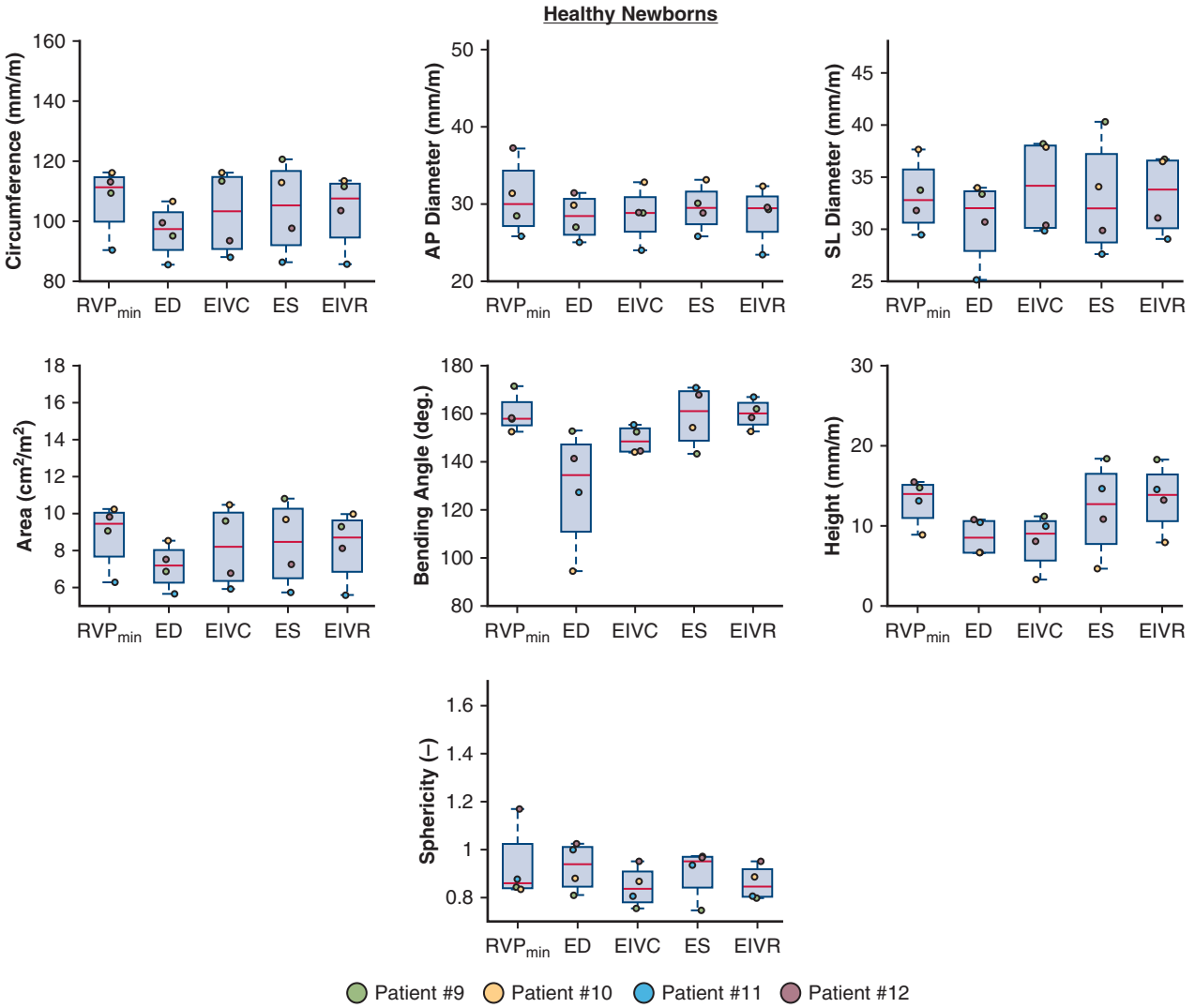

FIGURE 5. Key TV annulus clinical metrics for all healthy newborns (n = 4) at the selected time points over the cardiac cycle (*solid red line*: the median, the bounding box: the 25th to 75th percentiles, the *whiskers*: extension between the maximum and minimum nonoutlier datapoints). Individual patient data points at each time point are visualized with jittering for improved visual clarity. *TV*, Tricuspid valve; *RVP_{min}*, minimum right ventricular pressure; *ED*, end diastole; *EIVC*, end-isovolumetric contraction; *ES*, end systole; *EIVR*, end-isovolumetric relaxation; *SL*, septal-lateral; *AP*, anteroposterior.

the minimal strain in the anterior segment (<5% on average at all selected time points). For the strain rate, the largest changes were found at EIVC: posterior segment (5.2 ± 63.0%/s), anterior segment (60.9 ± 66.6%/s), and septal segment (–158.8 ± 96.1%/s). Finally, we observed a maximum change in the relative curvature for the posterior and anterior segments (±1.0 mm^{-1}), along with a ±2.0 mm^{-1} curvature change for the septal segment.

Differences Between Healthy and HLHS Newborns

We noted several key differences in TV annulus geometry between the newborns with HLHS and healthy newborns. First, D_{AP} and the annular circumference were larger for patients with HLHS at all 5 analyzed time points (35%-45% and 20%-30% larger, respectively; $.001 < P < .040$). Interestingly, however, D_{SL} was similar between the 2 groups ($.074 < P < .260$). These trends were similarly reflected in the annular area, wherein the area was significantly larger (44%-65%) for the patients with HLHS at all time points, except EIVC ($.002 < P < .060$). The sphericity was also significantly different between patient subgroups at all time points except ED ($.017 < P < .040$). Specifically, the healthy newborns exhibited an elliptical annulus with the major axis in the D_{SL} direction (ie, $D_{AP}/D_{SL} < 1$), whereas the patients with HLHS had an elliptical annulus at RVP_{min} (ie, $D_{AP}/D_{SL} > 1$) that became more circular during valve closure (ie, $D_{AP}/D_{SL} \approx 1$).

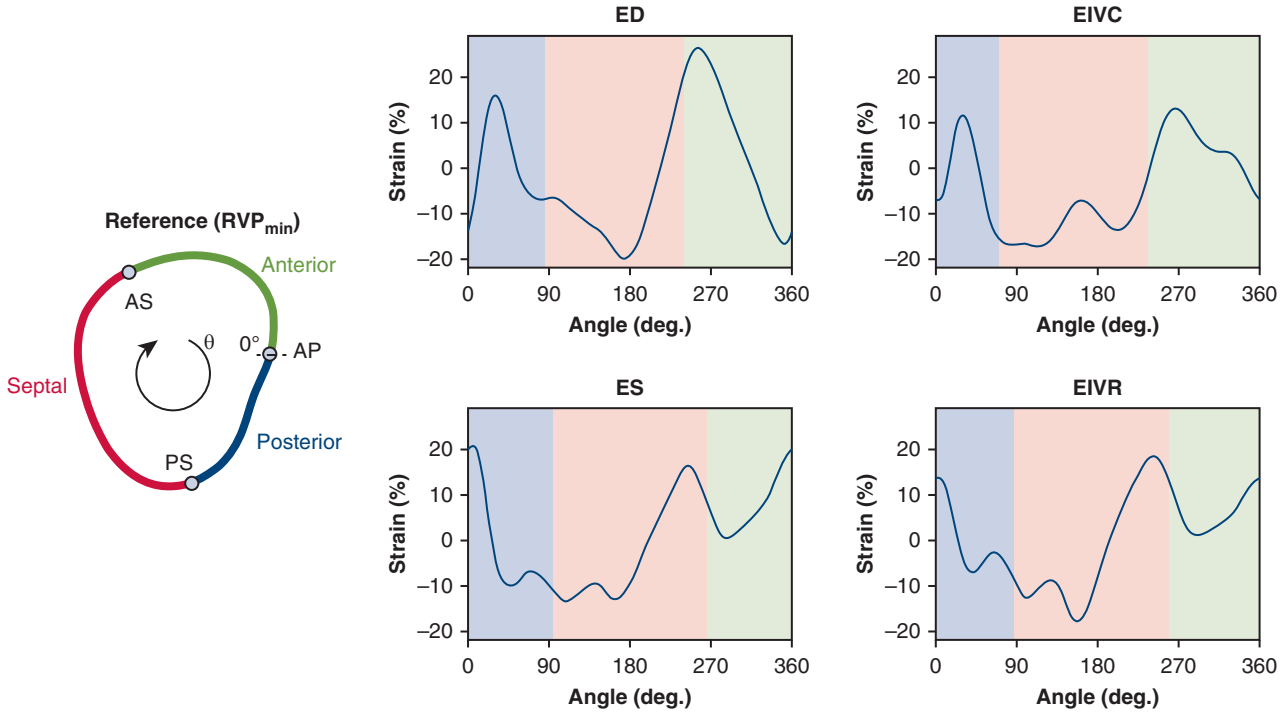

FIGURE 6. Spatial variations of the computed strain along the TV annulus circumference for a representative HLHS newborn (Patient #1) at the selected time points over the cardiac cycle, where the time instant $t_{RVP_{min}}$ was chosen as the reference configuration (RVP_{min}). Note that the 0° angle was aligned with the anteroposterior commissure. *TV*, Tricuspid valve; *HLHS*, hypoplastic left heart syndrome; *AS*, anteroseptal; *AP*, anteroposterior; *PS*, posteroseptal; *RVP_{min}*, minimum right ventricular pressure; *ED*, end diastole; *EIVC*, end-isovolumetric contraction; *ES*, end systole; *EIVR*, end-isovolumetric relaxation.

From the biomechanics standpoint, we did not observe as many significant differences between the newborns with HLHS and healthy newborns. For the strain, a significant difference was found in the anterior segment (HLHS vs healthy): $-0.1 \pm 2.6\%$ versus $-13.3 \pm 2.9\%$ at ED ($P = .010$), and $-1.7 \pm 3.0\%$ versus $6.8 \pm 0.9\%$ at end-isovolumetric relaxation ($P = .026$). This trend was partially reflected in the larger strain rate of 15%/s at ED for the healthy patients than the newborns with HLHS ($P = .011$). For curvature, significant differences were found for the septal segment at EIVC, ES ($P = .002$), anterior segment at RVP_{min}, ED ($.008 < P < .040$), and posterior segment at EIVC, ED, and ES ($.016 < P < .049$).

DISCUSSION

In this study, we presented a novel biomechanics-based framework for the analysis of dynamic valve annuli that we have preliminarily applied to elucidate the TV annular mechanics in neonates with HLHS. A complete understanding of the dynamic changes in the TV annulus biomechanics and geometric features will be integral in identifying patient conditions that are related to TR initiation and progression.

Comparisons Between Healthy Newborns and Newborns With HLHS

Comparing the newborns with HLHS and healthy newborns, we observed different annular geometries. Specifically, patients with HLHS had a larger circumference, area, and D_{AP} than the healthy cohort, along with different trends in sphericity over the cardiac cycle.

In contrast, the similarity in annular strain between healthy patients and patients with HLHS could have interesting implications for understanding the remodeling of the TV annulus in this unique congenital condition. For example, the HLHS-afflicted TV may adapt during embryonic developments to maintain similar homeostatic tissue strains as in the healthy (ie, non-HLHS) scenario. However, future studies are warranted to corroborate this postulation, which could include analyzing in utero echocardiograms of HLHS development. Also, the trends in annular strains could be related to the circumferential strains of the right ventricle, as shown to be similar between healthy newborns and newborns with HLHS.[29] It is worth noting that a previous study indicated that post-Norwood patients with HLHS had a reduced longitudinal strain of the right ventricle compared with the healthy patients, indicating the future development of TR and/or right ventricular dysfunction.[30]

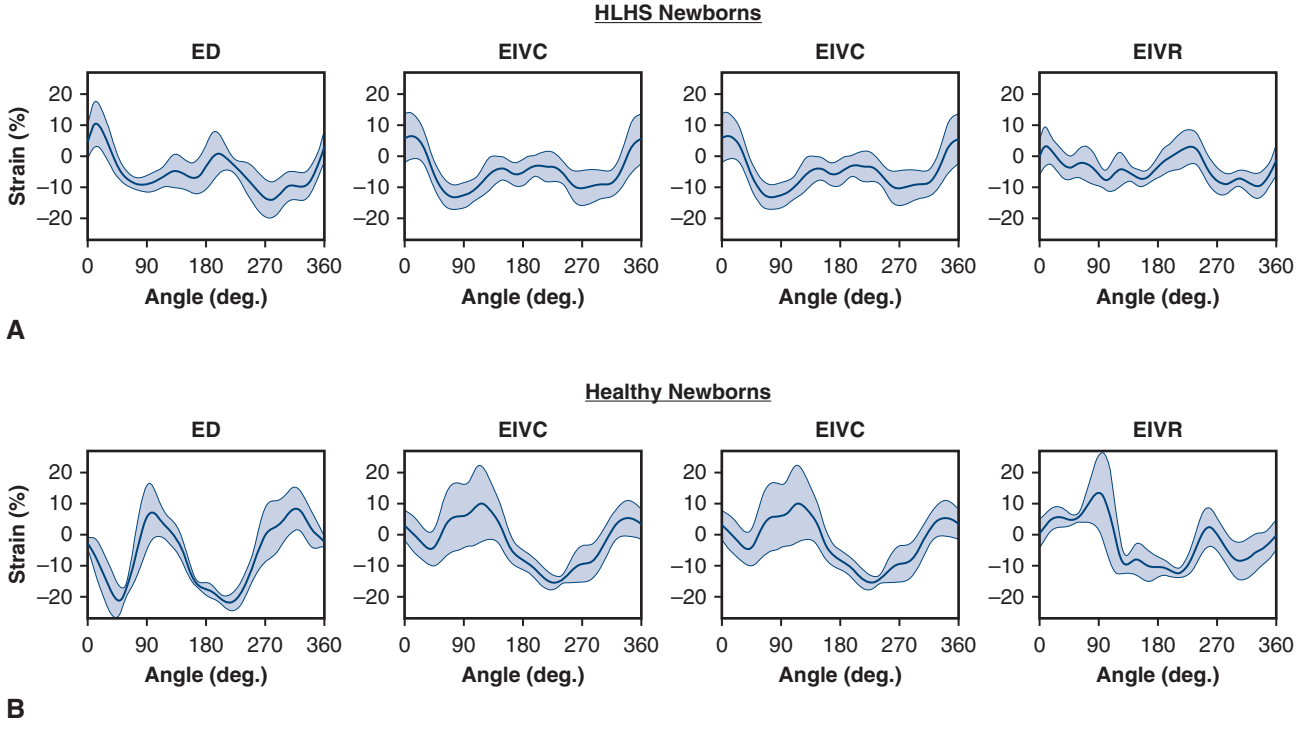

FIGURE 7. Spatial variations of the computed strain along the TV annulus circumference for (A) the studied 8 newborns with HLHS (n = 8), and (B) the 4 healthy newborns (n = 4) (*solid lines*: mean, *shaded regions*: standard error of the mean). Note that the 0° angle was aligned with the anteroposterior commissure. *TV*, Tricuspid valve; *HLHS*, hypoplastic left heart syndrome; *ED*, end diastole; *EIVC*, end-isovolumetric contraction; *EIVR*, end-isovolumetric relaxation.

Development of TR in HLHS Newborns

Previous investigators shed light on the distinct differences in the TV for newborns with HLHS with and without TR. It has been found that patients with HLHS with TR have (1) a larger annular area, (2) a lessened change in area during the cardiac cycle (TR, 12% vs no-TR, 20%),[11,12] (3) a flatter annulus with a reduced "active bending" (14° vs 27° changes in bending angle, TR vs no-TR),[6,12] and (4) heterogenous annular contractions, whereas in "normal" patients with HLHS, the contractions are homogenous.[12,15] While we were unable to enroll any patients with HLHS with TR in the present work, we may be able to observe the onset of TV anomalies as we track our patients in a future longitudinal study. For example, patient #8 had smaller changes in the annular area during the cardiac cycle (3%-13%) compared with others in the

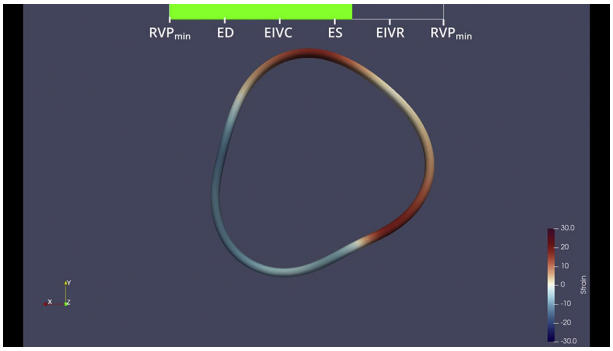

VIDEO 1. Change in the annular strain throughout the cardiac cycle for patient #1 with HLHS. Note that the TV annulus is visualized in an orientation similar to Figure 6. Video available at: https://www.jtcvs.org/article/S2666-2736(22)00069-9/fulltext.

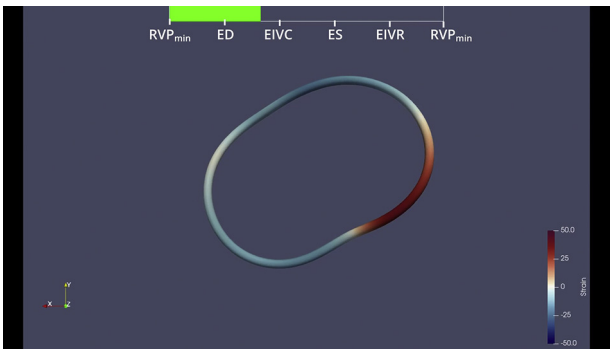

VIDEO 2. Change in the annular strain throughout the cardiac cycle for patient #2 with HLHS. Note that the TV annulus is visualized in an orientation similar to Figure 6. Video available at: https://www.jtcvs.org/article/S2666-2736(22)00069-9/fulltext.

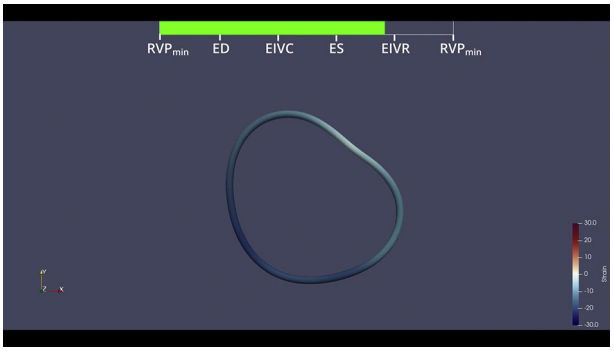

VIDEO 3. Change in the annular strain throughout the cardiac cycle for patient #3 with HLHS. Note that the TV annulus is visualized in an orientation similar to Figure 6. Video available at: https://www.jtcvs.org/article/S2666-2736(22)00069-9/fulltext.

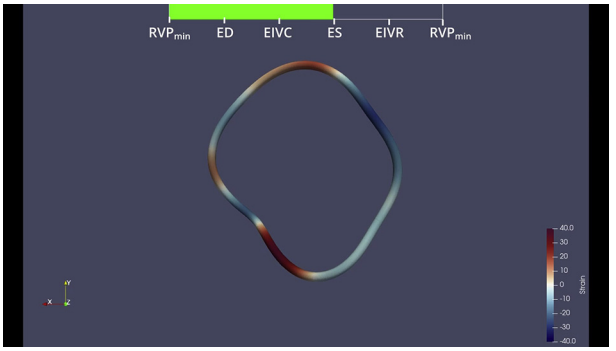

VIDEO 5. Change in the annular strain throughout the cardiac cycle for patient #5 with HLHS. Note that the TV annulus is visualized in an orientation similar to Figure 6. Video available at: https://www.jtcvs.org/article/S2666-2736(22)00069-9/fulltext.

cohort, which may serve as an indicator for potential TR initiation and development.

Comparisons to Previous TV Annulus Biomechanics Studies

While we can contextualize our annulus biomechanics findings regarding the previous in vitro animal studies and ex vivo heart pressurization systems, these studies analyze biventricular hearts. Between the biventricular and HLHS-afflicted hearts, the TV has numerous differences: (1) the TV is not designed to function with a circular annulus; (2) the septal–lateral contraction forces that maintain leaflet coaptation are reduced; and (3) ventricular dilation can cause papillary muscle shifting and a loss of leaflet coaptation.[12] Considering these differences, we observed strain magnitudes of ∼8%, on average at each time point, which were similar to those reported in other in vivo ovine animal studies using the sonomicrometry technique. For example, Malinowski and colleagues[31] incrementally cinched the ovine TV annulus and found annular strains increased from 20% to 40% with increased suturing strengths, whereas another study of the healthy ovine TV annulus observed peak strains of approximately 10%.[27] These findings were similar to another work perfusing ex vivo human hearts to identify peak strains of ∼10%.[32] The discrepancy in the observed peak strains may be attributed to the image acquisition methods (ie, interpolation with 8 sonocrystal locations vs 40-45 segmented locations in the present work), the differences in the ovine and the HLHS-afflicted hearts, or the use of in vivo versus ex vivo experimental methods.

Clinical Relevance and Translatability of the TV Annulus Pipeline

The development of this framework lays the foundation for improved patient diagnostics that can be used in refined clinical decisions and surgical planning. Using this pipeline, clinicians can receive the geometric and engineering-based analytics within an hour, demonstrating another benefit of

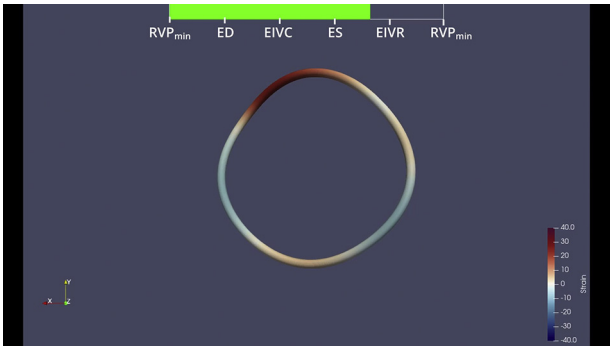

VIDEO 4. Change in the annular strain throughout the cardiac cycle for patient #4 with HLHS. Note that the TV annulus is visualized in an orientation similar to Figure 6. Video available at: https://www.jtcvs.org/article/S2666-2736(22)00069-9/fulltext.

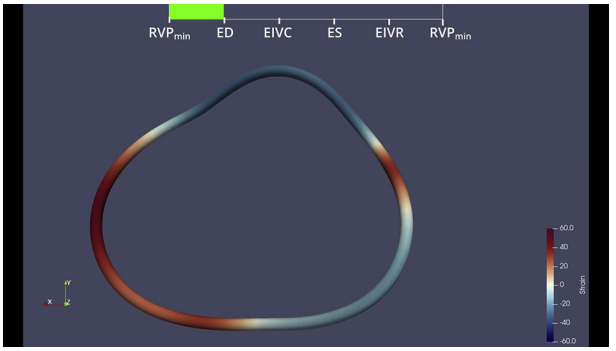

VIDEO 6. Change in the annular strain throughout the cardiac cycle for HLHS patient #6 with HLHS. Note that the TV annulus is visualized in an orientation similar to Figure 6. Video available at: https://www.jtcvs.org/article/S2666-2736(22)00069-9/fulltext.

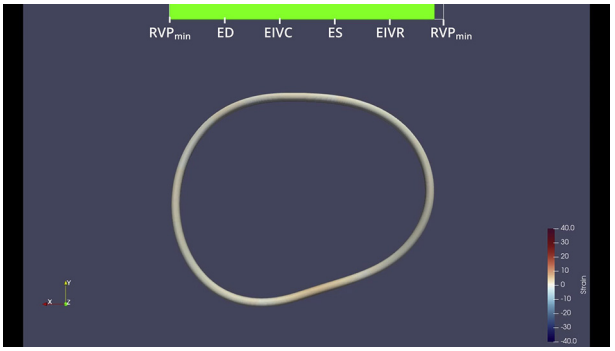

VIDEO 7. Change in the annular strain throughout the cardiac cycle for patient #7 with HLHS. Note that the TV annulus is visualized in an orientation similar to Figure 6. Video available at: https://www.jtcvs.org/article/S2666-2736(22)00069-9/fulltext.

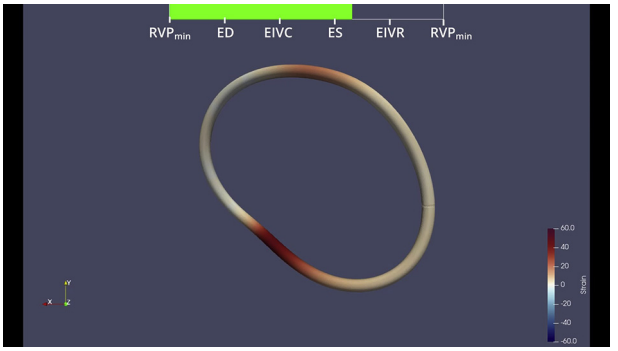

VIDEO 9. Change in the annular strain throughout the cardiac cycle for healthy patient #1 (ie, patient #9). Note that the TV annulus is visualized in an orientation similar to Figure 6. Video available at: https://www.jtcvs.org/article/S2666-2736(22)00069-9/fulltext.

our present work. While we opted to perform manual segmentation, semiautomated or deep learning-based automatic approaches for echocardiogram segmentation of the subvalvular components are a growing field of interest and could further improve the ease of use—a potential future extension.[18,33-35] With extensions of our TV analysis framework to include the leaflets and ventricle, further information on the unique biomechanics-based indicators can become available for surgical guidance such as the optimal timing of performing TV valvuloplasty repair.

Limitations and Future Extensions

There are a few limitations of the present work. First, we had a limited population size for our pilot investigation; thus, our findings are preliminary and should be interpreted in the correct context (ie, not be applied a larger population). Second, we were unable to identify trends in the development of TR in our HLHS cohort due to the limited available data from our retrospective patient enrollment. Third, there is a potential loss of local landmarks and features in the TV annulus due to the image-segmentation technique (ie, manual point placement or image resolution) or the moving least squares data fitting/smoothing algorithm. Nonetheless, the circumference changes observed in our study (up to 9% on average) were similar to those reported in the literature,[15,27,31] ensuring confidence in our analysis technique.

Future work includes investigating the changes in geometry and strains of the TV leaflets and other subvalvular structures, examining right ventricle function, and capturing the longitudinal changes in the TV annulus dynamics in individual patients using follow-up imaging data (eg, at 8 weeks vs 16 weeks of age, or at stage II/stage III palliation) to elucidate the time-evolving indicators of the initiation and progression of TR between the palliation stages. While the present work provides the foundation for understanding the TV annulus in patients with HLHS, the occurrence of TR is multifactorial, and all subvalvular

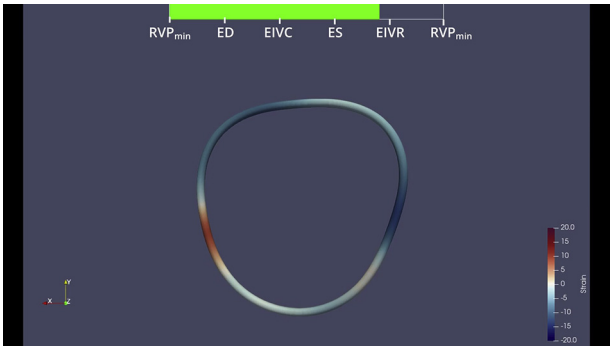

VIDEO 8. Change in the annular strain throughout the cardiac cycle for patient #8 with HLHS. Note that the TV annulus is visualized in an orientation similar to Figure 6. Video available at: https://www.jtcvs.org/article/S2666-2736(22)00069-9/fulltext.

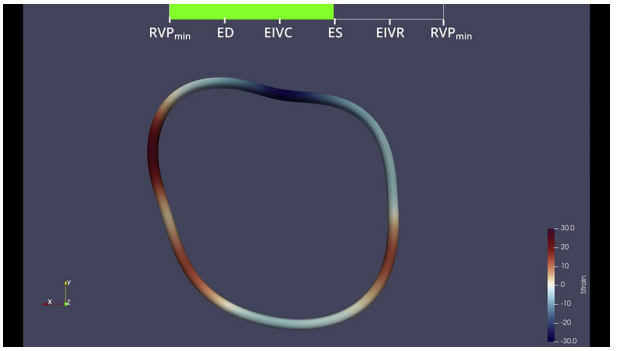

VIDEO 10. Change in the annular strain throughout the cardiac cycle for healthy patient #2 (ie, patient #10). Note that the TV annulus is visualized in an orientation similar to Figure 6. Video available at: https://www.jtcvs.org/article/S2666-2736(22)00069-9/fulltext.

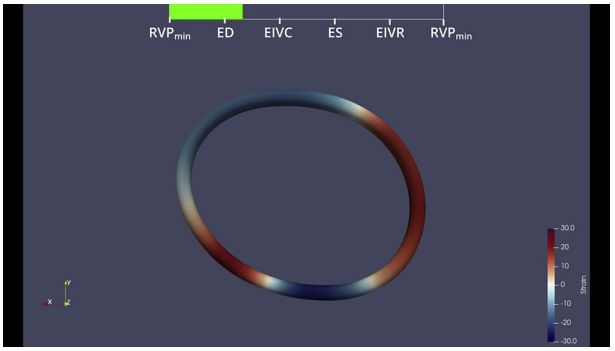

VIDEO 11. Change in the annular strain throughout the cardiac cycle for healthy patient #3 (ie, patient #11). Note that the TV annulus is visualized in an orientation similar to Figure 6. Video available at: https://www.jtcvs.org/article/S2666-2736(22)00069-9/fulltext.

components can likely contribute to the manifestation of the comorbidity.

CONCLUSIONS

We have presented a comprehensive patient-specific TV annulus analysis pipeline that is capable of quantifying both the biomechanical and geometric indices, including annular tissue strains from the 4-dimensional echocardiograms. We found that newborns with HLHS had annular strains of ∼8%, on average, and a more circular annulus during the heart valve contraction. In addition, the HLHS TV annulus was significantly larger than the healthy one, while maintaining similar strains. Application of these techniques to a larger patient cohort in future studies may inform the optimal timing and selection of TV surgical intervention for the challenging HLHS population.

Conflict of Interest Statement

The authors reported no conflicts of interest.

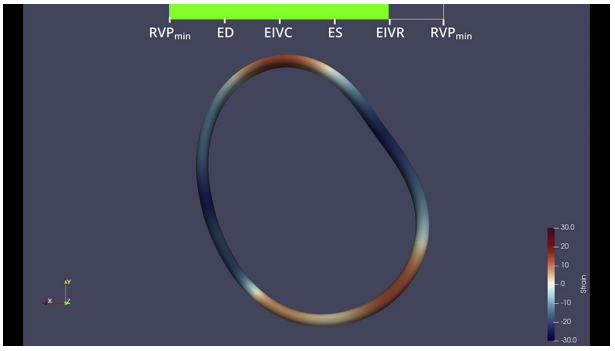

VIDEO 12. Change in the annular strain throughout the cardiac cycle for healthy patient #4 (ie, patient #12). Note that the TV annulus is visualized in an orientation similar to Figure 6. Video available at: https://www.jtcvs.org/article/S2666-2736(22)00069-9/fulltext.

The *Journal* policy requires editors and reviewers to disclose conflicts of interest and to decline handling or reviewing manuscripts for which they may have a conflict of interest. The editors and reviewers of this article have no conflicts of interest.

References

1. Mai CT, Isenburg JL, Canfield MA, Meyer RE, Correa A, Alverson CJ, et al. National population-based estimates for major birth defects, 2010-2014. *Birth Defects Res*. 2019;111:1420-35.
2. Hamzah M, Othman HF, Baloglu O, Aly H. Outcomes of hypoplastic left heart syndrome: analysis of national inpatient sample database 1998-2004 versus 2005-2014. *Eur J Pediatr*. 2020;179:309-16.
3. Pundi KN, Johnson JN, Dearani JA, Pundi KN, Li Z, Hinck CA, et al. 40-year follow-up after the Fontan operation: long-term outcomes of 1,052 patients. *J Am Coll Cardiol*. 2015;66:1700-10.
4. Poh CL, d'Udekem Y. Life after surviving Fontan surgery: a meta-analysis of the incidence and predictors of late death. *Heart Lung Circ*. 2018;27:552-9.
5. Ono M, Boethig D, Goerler H, Lange M, Westhoff-Bleck M, Breymann T. Clinical outcome of patients 20 years after Fontan operation—effect of fenestration on late morbidity. *Eur J Cardiothorac Surg*. 2006;30:923-9.
6. Colen T, Kutty S, Thompson RB, Tham E, Mackie AS, Li L, et al. Tricuspid valve adaptation during the first interstage period in hypoplastic left heart syndrome. *J Am Soc Echocardiogr*. 2018;31:624-33.
7. Kutty S, Colen T, Thompson RB, Tham E, Li L, Vijarnsorn C, et al. Tricuspid regurgitation in hypoplastic left heart syndrome: mechanistic insights from 3-dimensional echocardiography and relationship with outcomes. *Circ Cardiovasc Imaging*. 2014;7:765-72.
8. Ohye RG, Gomez CA, Goldberg CS, Graves HL, Devaney EJ, Bove EL. Tricuspid valve repair in hypoplastic left heart syndrome. *J Thorac Cardiovasc Surg*. 2004;127:465-72.
9. Alsoufi B, Sinha R, McCracken C, Figueroa J, Altin F, Kanter K. Outcomes and risk factors associated with tricuspid valve repair in children with hypoplastic left heart syndrome. *Eur J Cardiothorac Surg*. 2018;54:993-1000.
10. Muntaner CD, King G, Zannino D, Alphonso N, Finucance K, Winlaw D, et al. Poor late outcomes after tricuspid valve repair in a single ventricle: experience of 103 patients. *Ann Thorac Surg*. 2021;111:987-94.
11. Takahashi K, Inage A, Rebeyka IM, Ross DB, Thompson RB, Mackie AS, et al. Real-time 3-dimensional echocardiography provides new insight into mechanisms of tricuspid valve regurgitation in patients with hypoplastic left heart syndrome. *Circulation*. 2009;120:1091.
12. Nii M, Guerra V, Roman KS, Macgowan CK, Smallhorn JF. Three-dimensional tricuspid annular function provides insight into the mechanisms of tricuspid valve regurgitation in classic hypoplastic left heart syndrome. *J Am Soc Echocardiogr*. 2006;19:391-402.
13. Ono M, Mayr B, Burri M, Piber N, Röhlig C, Strbad M, et al. Tricuspid valve repair in children with hypoplastic left heart syndrome: impact of timing and mechanism on outcome. *Eur J Cardiothorac Surg*. 2020;57:1083-90.
14. Bharucha T, Honjo O, Seller N, Atlin C, Redington A, Caldarone CA, et al. Mechanisms of tricuspid valve regurgitation in hypoplastic left heart syndrome: a case-matched echocardiographic–surgical comparison study. *Eur Heart J Cardiovasc Imaging*. 2013;14:135-41.
15. Nguyen AV, Lasso A, Nam HH, Faerber J, Aly AH, Pouch AM, et al. Dynamic three-dimensional geometry of the tricuspid valve annulus in hypoplastic left heart syndrome with a Fontan circulation. *J Am Soc Echocardiogr*. 2019;32:655-66.e613.
16. Laohachai K, Winlaw D, Sholler G, Veerappan S, Cole A, Ayer J. The degree of left ventricular hypoplasia is associated with tricuspid regurgitation severity in infants with hypoplastic left heart syndrome. *Pediatr Cardiol*. 2019;40:1035-40.
17. Ricci M, Mohapatra B, Urbiztondo A, Birusingh RJ, Morgado M, Rodriguez MM, et al. Differential changes in TGF-β/BMP signaling pathway in the right ventricular myocardium of newborns with hypoplastic left heart syndrome. *J Card Fail*. 2010;16:628-34.
18. Pouch AM, Aly AH, Lasso A, Nguyen AV, Scanlan AB, McGowan FX, et al. Image segmentation and modeling of the pediatric tricuspid valve in hypoplastic left heart syndrome. *Funct Imaging Model Heart*. 2017;10263:95-105.
19. Scanlan AB, Nguyen AV, Ilina A, Lasso A, Cripe L, Jegatheeswaran A, et al. Comparison of 3D echocardiogram-derived 3D printed valve models to molded

models for simulated repair of pediatric atrioventricular valves. *Pediatr Cardiol*. 2018;39:538-47.
20. Fedorov A, Beichel R, Kalpathy-Cramer J, Finet J, Fillion-Robin J-C, Pujol S, et al. 3D Slicer as an image computing platform for the quantitative imaging network. *Magn Reson Imaging*. 2012;30:1323-41.
21. Rausch MK, Bothe W, Kvitting J-PE, Göktepe S, Miller DC, Kuhl E. *In vivo* dynamic strains of the ovine anterior mitral valve leaflet. *J Biomech*. 2011;44:1149-57.
22. Eckert CE, Zubiate B, Vergnat M, Gorman JH III, Gorman RC, Sacks MS. *In vivo* dynamic deformation of the mitral valve annulus. *Ann Biomed Eng*. 2009;37:1757-71.
23. Belytschko T, Krongauz Y, Organ D, Fleming M, Krysl P. Meshless methods: an overview and recent developments. *Comput Methods Appl Mech Eng*. 1996;139:3-47.
24. Chen J-S, Pan C, Wu C-T, Liu WK. Reproducing kernel particle methods for large deformation analysis of non-linear structures. *Comput Methods Appl Mech Eng*. 1996;139:195-227.
25. Khoiy KA, Asgarian KT, Loth F, Amini R. Dilation of tricuspid valve annulus immediately after rupture of chordae tendineae in ex-vivo porcine hearts. *PLoS One*. 2018;13:e0206744.
26. Rausch MK, Tibayan FA, Ingels NB, Miller DC, Kuhl E. Mechanics of the mitral annulus in chronic ischemic cardiomyopathy. *Ann Biomed Eng*. 2013;41:2171-80.
27. Rausch MK, Malinowski M, Wilton P, Khaghani A, Timek TA. Engineering analysis of tricuspid annular dynamics in the beating ovine heart. *Ann Biomed Eng*. 2018;46:443-51.
28. Haycock GB, Schwartz GJ, Wisotsky DH. Geometric method for measuring body surface area: a height-weight formula validated in infants, children, and adults. *J Pediatr*. 1978;93:62-6.
29. Petko C, Uebing A, Furck A, Rickers C, Scheewe J, Kramer H-H. Changes of right ventricular function and longitudinal deformation in children with hypoplastic left heart syndrome before and after the Norwood operation. *J Am Soc Echocardiogr*. 2011;24:1226-32.
30. Pettersen E, Helle-Valle T, Edvardsen T, Lindberg H, Smith H-J, Smevik B, et al. Contraction pattern of the systemic right ventricle. *J Am Coll Cardiol*. 2007;49:2450-6.
31. Malinowski M, Schubert H, Wodarek J, Ferguson H, Eberhart L, Langholz D, et al. Tricuspid annular geometry and strain after suture annuloplasty in acute ovine right heart failure. *Ann Thorac Surg*. 2018;106:1804-11.
32. Malinowski M, Jazwiec T, Goehler M, Quay N, Bush J, Jovinge S, et al. Sonomicrometry-derived 3-dimensional geometry of the human tricuspid annulus. *J Thorac Cardiovasc Surg*. 2018;157:1452-61.
33. Pouch AM, Xu C, Yushkevich PA, Jassar AS, Vergnat M, Gorman JH III, et al. Semi-automated mitral valve morphometry and computational stress analysis using 3D ultrasound. *J Biomech*. 2012;45:903-7.
34. Pouch AM, Wang H, Takabe M, Jackson BM, Sehgal CM, Gorman JH III, et al. Automated segmentation and geometrical modeling of the tricuspid aortic valve in 3D echocardiographic images. *Med Image Comput Comput Assist Interv*. 2013;16(Pt 1):485-92.
35. Herz C, Pace DF, Nam HH, Lasso A, Dinh P, Flynn M, et al. Segmentation of tricuspid valve leaflets from transthoracic 3D echocardiograms of children with hypoplastic left heart syndrome using deep learning. *Front Cardiovasc Med*. 2021;8:735587.

Key Words: mechanical strains, image segmentation, tricuspid valve geometry, congenital heart defect, transthoracic echocardiographic imaging

APPENDIX 1. DETAILS ON THE MOVING LEAST-SQUARES CURVE FITTING AND DETERMINATION OF GEOMETRY- AND ENGINEERING MECHANICS–BASED ANALYSES FOR THE TRICUSPID VALVE (TV) ANNULUS

The (X, Y, Z) coordinates from the TV annulus point clouds were imported to MATLAB (MathWorks). Annulus curve fitting was performed using a moving least-squares algorithm to generate 300 material points to determine geometric measurements: the anteroposterior septal-lateral diameters, the annular height, the bending angle, the circumference, the annular area, and the sphericity and biomechanical metrics (eg, strain, strain rate, and relative curvature).

Let C be the TV annulus curve parametrized by the moving least-squares functions in a cylindrical coordinate system (r, θ, z):

$$C(X,Y,Z) = \left(\sum_{J=1}^{NP} \Psi_J(\theta) r_J,\ \theta,\ \sum_{J=1}^{NP} \Psi_J(\theta) z_J \right), \quad \text{(A.1)}$$

Where the TV annulus is represented by NP discrete points associated with their unknown r_J and z_J coordinates and the moving least-squares shape functions Ψ_J. The transformation between the cylindrical and Cartesian coordinate systems follows: $X = r\cos\theta$, $Y = r\sin\theta$, and $Z = z$.

According to Belytschko and colleagues[23] and Chen and colleagues,[24] the 1-dimensional moving least-squares shape functions are constructed by:

$$\Psi_J(\theta) = \mathbf{H}^T(0)\mathbf{M}^{-1}(\theta)\mathbf{H}(\theta-\theta_J)\phi(\theta-\theta_J;w), \quad \text{(A.2)}$$

Herein, $\mathbf{H}^T(\theta-\theta_J) = [1, \theta-\theta_J, \cdots, (\theta-\theta_J)^N]$ is the basis function up to a monomial order of N, Φ is the window function with a support of w, and $\mathbf{M}(\theta)$ is the moment matrix defined as:

$$\mathbf{M}(\theta) = \sum_{K=1}^{NP} \mathbf{H}^T(\theta-\theta_K)\mathbf{H}(\theta-\theta_K)\phi(\theta-\theta_K;w). \quad \text{(A.3)}$$

In this study, we chose $NP = 9$, a quadratic basis function, ie, $N = 2$, a cubic B-spline function for Φ, and a support of $w = 3.25$ to parametrize the TV annulus curve (ie, a periodic curve with $\theta = 0^\circ - 360^\circ$) via standard linear least-squares regression with respect to the segmented 3-dimensional point cloud data (Figure 3, *A*). After the fitted curve was obtained, 300 uniformly spaced material points were generated in the θ coordinate for the subsequent analyses.

The biomechanical metrics were determined using the material points from the fitted annulus curve. Herein, we defined RVP_{min} as the reference configuration (Ω_0), as it is the time point in the cardiac cycle closest to a *stress-free* reference configuration.[26] The TV annulus strains, associated with each material point i located at (X_i, Y_i, Z_i), were computed by $\varepsilon_i = s_i^t/s_i^0$, where the superscripts 0 and t denote the reference Ω_0 and deformed states Ω_t, respectively. After the TV annulus strains were determined, the strain rate between any 2 time points t_1 and t_2 was calculated by $\dot{\varepsilon}_i = \Delta s_i/\Delta t = (s_i^{t_2} - s_i^{t_1})/(t_2 - t_1)$. To further gain insight into the geometry of the dynamic TV annulus, we also calculated the curvature by using the first- and second-order derivatives ($\mathbf{d}^{(1)}$ and $\mathbf{d}^{(2)}$) associated with the annulus curve[27]:

$$\kappa_i = \frac{\left|\mathbf{d}^{(1)}(X,Y,Z)_i \times \mathbf{d}^{(2)}(X,Y,Z)_i\right|}{\left|\mathbf{d}^{(1)}(X,Y,Z)_i\right|^3}. \quad \text{(A.4)}$$

In addition, we determined the relative curvature as the difference in curvature between the reference configuration and the subsequent time points (ie, $\kappa_{i,0} - \kappa_{i,t}$).

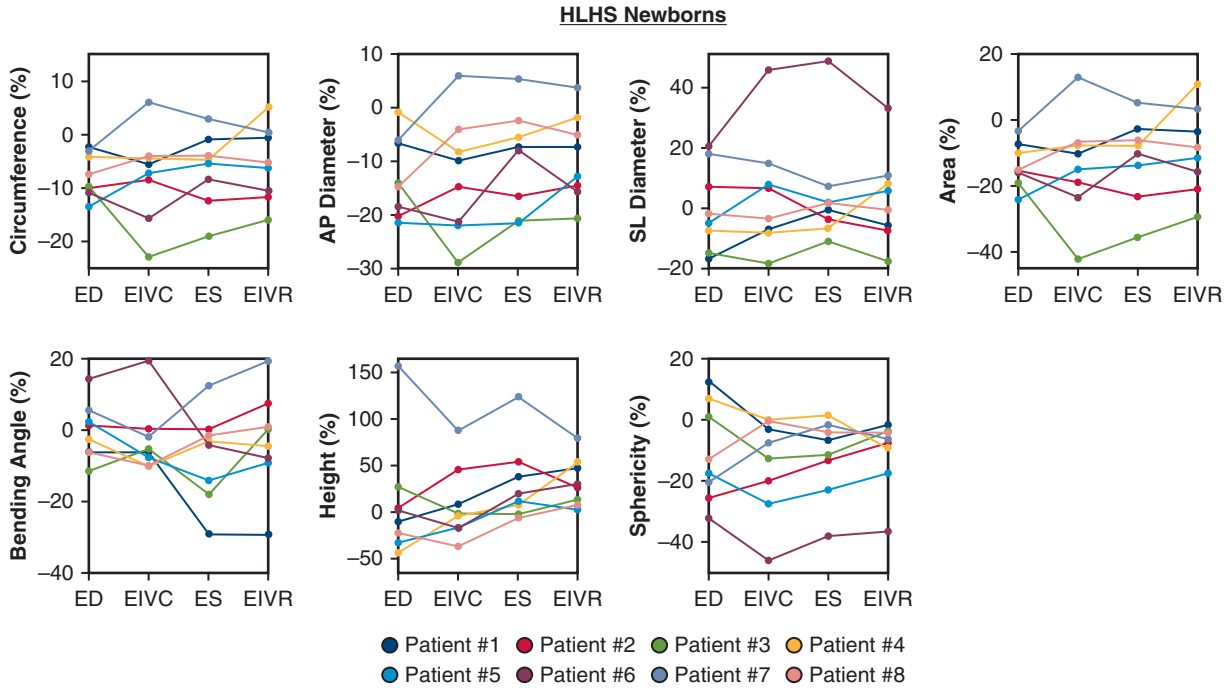

FIGURE E1. Percentage changes in the TV annulus clinical metrics for the HLHS newborns (n = 8) at the selected time points over the cardiac cycle. *TV*, Tricuspid valve; *HLHS*, hypoplastic left heart syndrome; *ED*, end diastole; *EIVC*, end-isovolumetric contraction; *ES*, end systole; *EIVR*, end-isovolumetric relaxation; *AP*, anteroposterior; *SL*, septal-lateral.

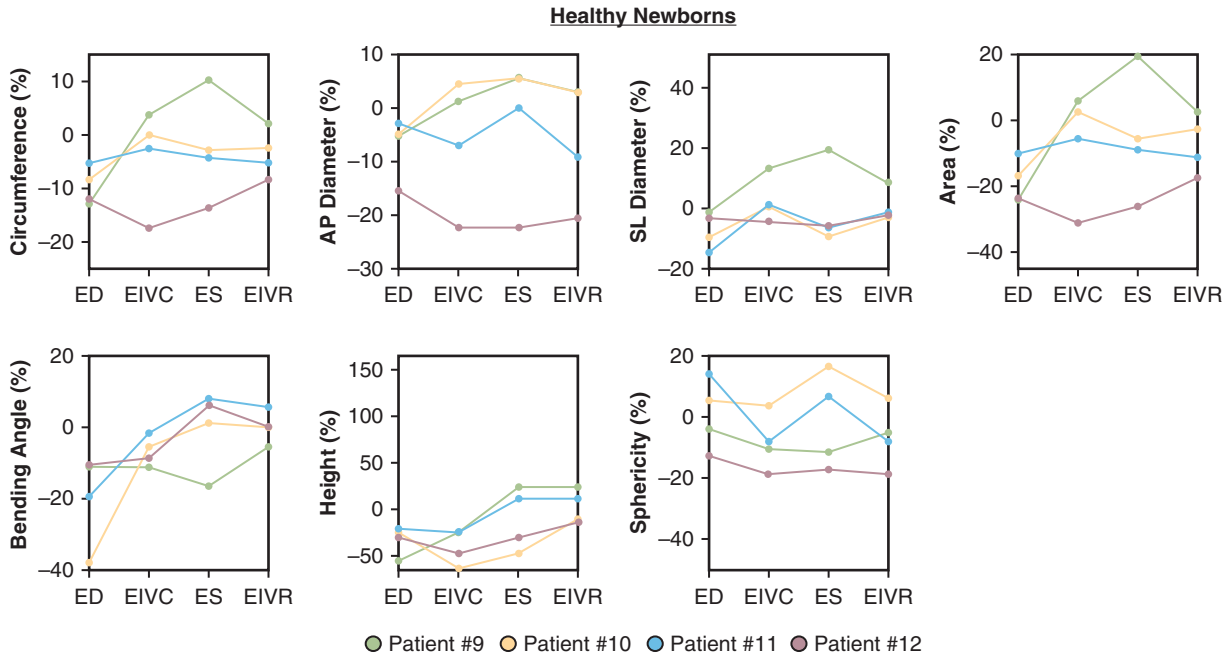

FIGURE E2. Percentage changes in the TV annulus clinical metrics for the healthy newborns (n = 4) at the selected time points over the cardiac cycle. *TV*, Tricuspid valve; *ED*, end diastole; *EIVC*, end-isovolumetric contraction; *ES*, end systole; *EIVR*, end-isovolumetric relaxation; *AP*, anteroposterior; *SL*, septal-lateral.

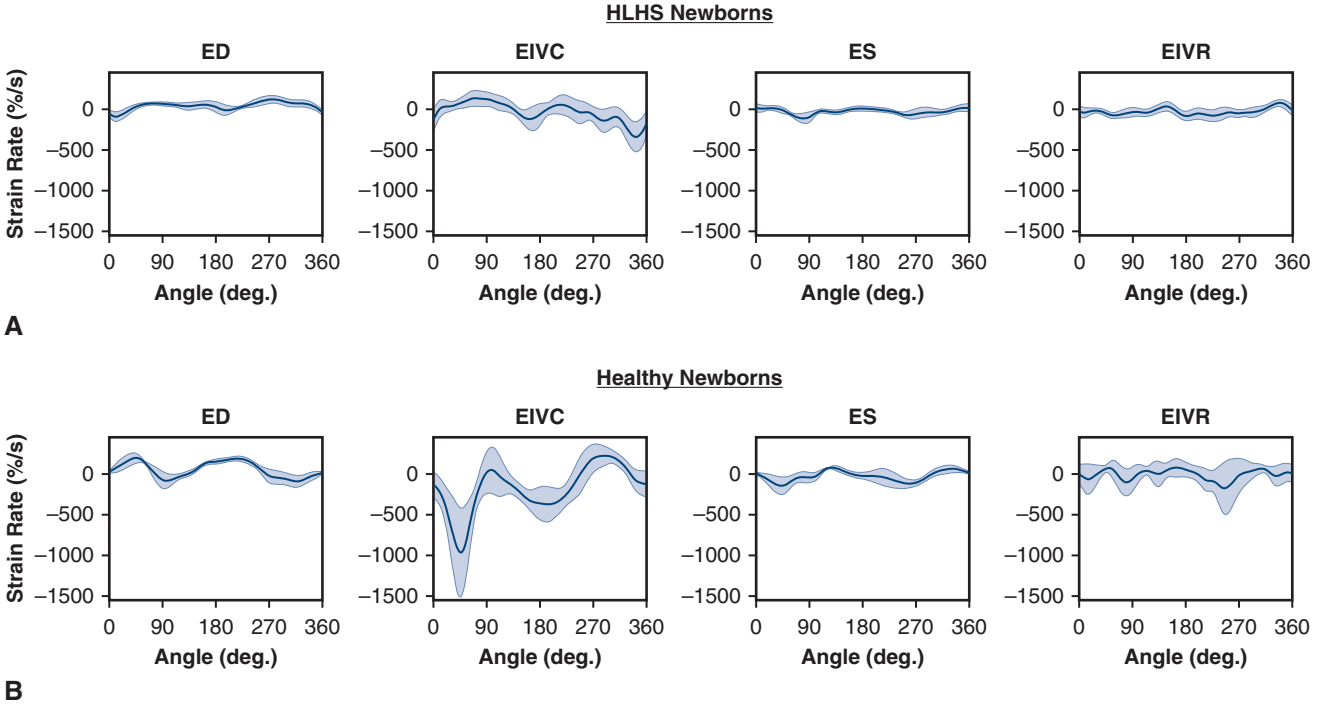

FIGURE E3. Spatial variations of the computed strain rate along the TV annulus circumference for (A) the studied 8 newborns with HLHS (n = 8), and (B) the 4 healthy newborns (n = 4) (*solid lines*: mean, *shaded regions*: standard error of the mean). Note that the 0° angle was aligned with the anteroposterior commissure. *TV*, Tricuspid valve; *HLHS*, hypoplastic left heart syndrome; *ED*, end diastole; *EIVC*, end-isovolumetric contraction; *ES*, end systole; *EIVR*, end-isovolumetric relaxation.

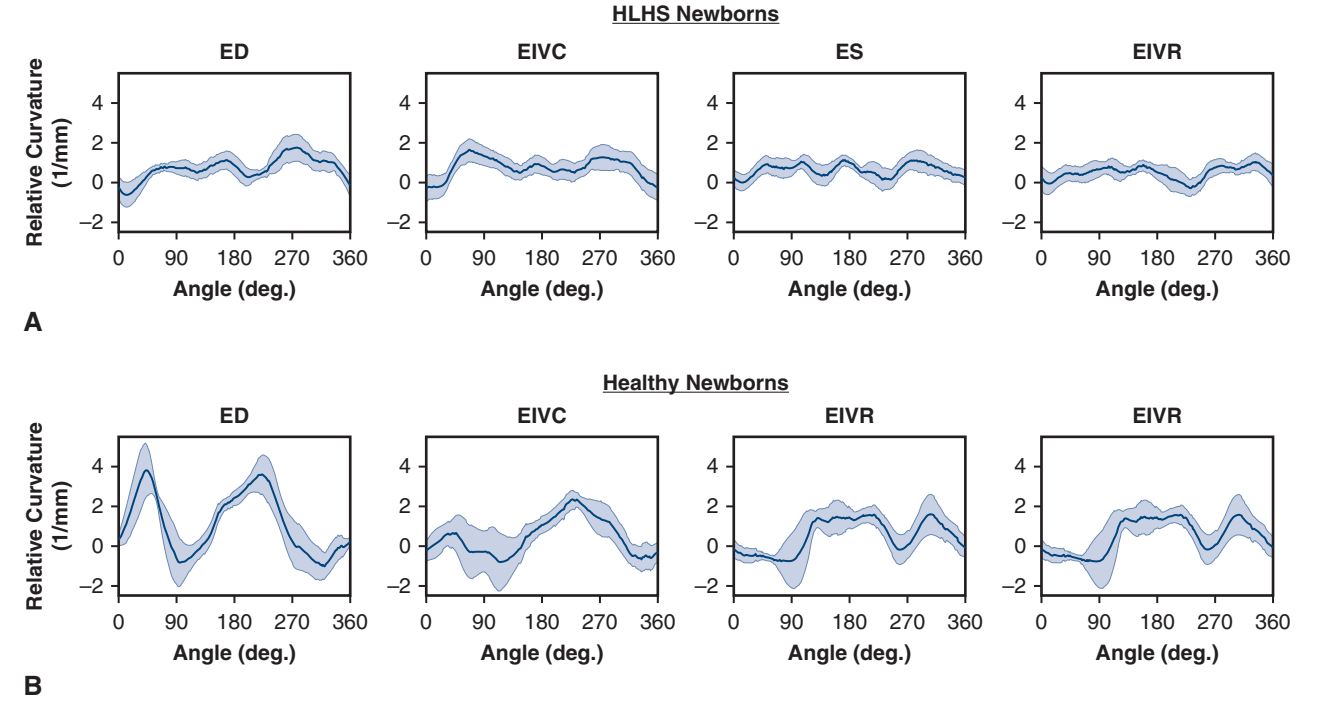

FIGURE E4. Spatial variations of the computed relative curvature along the TV annulus circumference for (A) the studied 8 newborns with HLHS (n = 8), and (B) the 4 healthy newborns (n = 4) (*solid lines*: mean, *shaded regions*: standard error of the mean). Note that the 0° angle was aligned with the anteroposterior commissure. *TV*, Tricuspid valve; *HLHS*, hypoplastic left heart syndrome; *ED*, end diastole; *EIVC*, end-isovolumetric contraction; *ES*, end systole; *EIVR*, end-isovolumetric relaxation.